Surface effects in x-ray absorption spectra of lanthanides: Focus on strongly correlated cerium materials

D. Yu. Usachov,[1,2,*] K. A. Bokai,[1,2] G. Poelchen,[3] V. S. Stolyarov,[2,4] A. V. Fedorov,[5] K. Kliemt,[6] S. Khim,[7] N. Caroca-Canales,[7] C. Krellner,[6] and D. V. Vyalikh[8,9,10,†]

[1]*St. Petersburg State University, 7/9 Universitetskaya nab., St. Petersburg 199034, Russia*
[2]*Moscow Institute of Physics and Technology, Institute Lane 9, Dolgoprudny 141701, Russia*
[3]*Institut für Festkörper- und Materialphysik, Technische Universität Dresden, 01069 Dresden, Germany*
[4]*National University of Science and Technology MISIS, Moscow 119049, Russia*
[5]*Helmholtz-Zentrum Berlin für Materialien und Energie, Albert-Einstein-Straße 15, 12489 Berlin, Germany*
[6]*Kristall- und Materiallabor, Physikalisches Institut, Goethe-Universität Frankfurt, Max-von-Laue Strasse 1, D-60438 Frankfurt am Main, Germany*
[7]*Max Planck Institute for Chemical Physics of Solids, 01187 Dresden, Germany*
[8]*Donostia International Physics Center (DIPC), 20018 Donostia/San Sebastián, Basque Country, Spain*
[9]*University of the Basque Country UPV/EHU, 20018 Donostia/San Sebastián, Spain*
[10]*IKERBASQUE, Basque Foundation for Science, 48013 Bilbao, Spain*

(Received 24 March 2025; revised 29 May 2025; accepted 26 June 2025; published 14 July 2025)

Lanthanide (Ln) materials are widely studied using x-ray absorption spectroscopy (XAS), primarily at the Ln $3d$ edge, with less attention given to the $4d$ edge. Spectral features are usually analyzed in relation to bulk properties with surface effects rarely considered. In this study, we explore surface phenomena and their impact on XAS spectra, using as examples the antiferromagnetic (AFM) Kondo lattice $CeRh_2Si_2$, where we thoroughly examine both the $3d$ and $4d$ edges, and AFM $LnRh_2Si_2$ (Ln = Tm, Tb, and Pr), where our focus is primarily on the $3d$ edge. We observe significant contributions from surface effects in the $3d$ XAS spectra, even when measured in the total electron yield regime. We find evidence of Ce $4f$ moment reorientation at the Ce-terminated surface of $CeRh_2Si_2$, linked to changes in the crystal electric field at the surface. By modeling the Ce $3d$ and $4d$ XAS spectra, we not only distinguish between surface and bulk properties but also reveal the fine multiplet structure and the characteristic shape of the giant resonance associated with $|M_J\rangle$ states. These findings provide insights into $4f$-derived surface phenomena and their distinction from bulk electronic properties, while also emphasizing the general importance of surface sensitivity in XAS measurements of Ln materials.

DOI: 10.1103/blg4-bxl5

I. INTRODUCTION

X-ray absorption spectroscopy is a powerful tool for investigating lanthanide (Ln) -based materials [1], particularly through the analysis of the Ln $4d \rightarrow 4f$ transitions and, more frequently, the $3d \rightarrow 4f$ absorption edges of Ln atoms [2]. From such measurements, essential information about the properties of lanthanides in the materials can be obtained, including their local coordination environments and crystal electric field (CEF), electronic configurations, oxidation state, and local symmetry as well as hybridization between strongly localized $4f$ electrons and itinerant states [3–5]. These insights are crucial for understanding the fundamental electronic structure and magnetic properties of Ln compounds [6]. Among these, intermetallics with unstable valence, such as those containing Ce, Eu, or Yb, have traditionally received significant attention and serve as prototypes for strongly correlated electron systems, revealing a wealth of extraordinary phenomena [7,8]. In the case of Ce-based compounds, information derived from Ce $3d$ edge XAS spectra, acquired in total electron yield (TEY) mode, is typically interpreted in the context of the bulk properties and phenomena of these materials [9–14]. However, the contribution from surface-related Ce atoms to the obtained XAS signal at the $3d$ edge is often overlooked. This issue extends beyond Ce systems to other lanthanide materials, where similar investigations remain unaddressed, leaving their surface properties largely unexplored in XAS experiments.

In recent studies of several $LnRh_2Si_2$ antiferromagnetic (AFM) materials with the $ThCr_2Si_2$ structure, we demonstrated how lanthanide atoms near the surface exhibit different properties than those in the bulk. Using $4f$-photoemission spectroscopy, we analyzed the line shape of the Ln $4f$ multiplet [15–17] and, later, XAS measurements at the Ln $4d$ edge [18] confirmed that surface-related modifications in the CEF can lead to significant reorientation of the $4f$ moments compared to the bulk. It is also worth noting that a similar reorientation of $4f$ moments, driven by surface-induced changes in the CEF, has been intensively discussed in the theoretical community in recent years for materials such as $Nd_2Fe_{14}B$ and $SmFe_{12}$ [19–21].

*Contact author: dmitry.usachov@spbu.ru
†Contact author: denis.vyalikh@dipc.org

 ©2025 American Physical Society

In this study, we extend our focus to Ce-based systems, with $CeRh_2Si_2$ as a representative example. The well-studied antiferromagnetic (AFM) Kondo lattice $CeRh_2Si_2$ ($T_N = 38$ K, $T_K \approx 30$ K) is particularly interesting due to its rich phase diagram, where antiferromagnetic order and unconventional superconductivity coexist in close proximity [22–26]. Given that $CeRh_2Si_2$ shares the same crystal structure as other $LnRh_2Si_2$ compounds [15–18], it is reasonable to expect that Ce $4f$ moments at its Ce-terminated surface might exhibit similar reorientation relative to the bulk. Since Ce-based materials are extensively studied using XAS at both the $3d$ and $4d$ edges, it is crucial to assess the extent to which surface-related properties influence the XAS signal and how they can be distinguished from bulk contributions. This is particularly relevant for TEY mode measurements, which are usually used to probe bulk properties. Our previous investigations of $CeRh_2Si_2$ revealed fine spectral features near the Fermi level (E_F) associated with CEF-split $4f$ states [27] and differences in Kondo-related temperature scales at the surface and in the bulk [28].

Based on these findings, we present a comprehensive study combining experimental XAS measurements at the Ce $3d$ and $4d$ edges with spectral modeling for $CeRh_2Si_2$. By examining both Ce- and Si-terminated surfaces, as in our previous work [27,28], we demonstrate that surface-related features are clearly distinguishable in Ce $3d$ XAS spectra, even in TEY mode, emphasizing the need to separate surface and bulk contributions. Our analysis reveals that Ce $4f$ moments at the Ce-terminated surface undergo reorientation due to modifications in the CEF, demonstrating the importance of accounting for surface effects when extracting bulk information. Additionally, we present XAS measurements in partial electron yield (PEY) mode, along with modeling for $TmRh_2Si_2$, $PrRh_2Si_2$, and $TbRh_2Si_2$, broadening the scope of this discussion on surface effects in XAS studies.

II. EXPERIMENT

XAS measurements were performed at the FlexPES [29] beamline of MAX IV, the Swedish national synchrotron radiation facility. The analytical chamber of the experimental station at FlexPES is equipped with a home-developed microchannel plate detector featuring a selectable retardation voltage, enabling XAS measurements in partial electron yield (PEY) regime. Combined with the TEY regime, this setup allows for tuning the sensitivity from bulklike to more surface-sensitive detection. The XAS spectra are presented without noise filtering. The energy step was 0.1 eV for the $3d$ and 0.05 eV for the $4d$ XAS spectra. High-quality single-crystalline samples of $LnRh_2Si_2$, crystallizing in the body-centered tetragonal $ThCr_2Si_2$ structure [30], were cleaved *in situ* under ultrahigh vacuum conditions, with a base pressure better than 1×10^{-10} mbar. Momentum-resolved photoemission measurements (ARPES), performed immediately after cleavage, enabled straightforward identification of either a Ln-terminated or Si-terminated surface [31]. The latter was established by the observation of a sharp spectral pattern of a surface state residing in the projected gap around the $\overline{\mathrm{M}}$ point of the surface Brillouin zone. This surface state disappears for the Ln-terminated surface [32–35]. Once the sample surface was accurately characterized, XAS spectra were acquired using horizontally polarized photons at normal incidence. The energy resolution in XAS measurements was better than 15 meV for the Ln $4d$ edge and better than 230 meV for the Ln $3d$ edge.

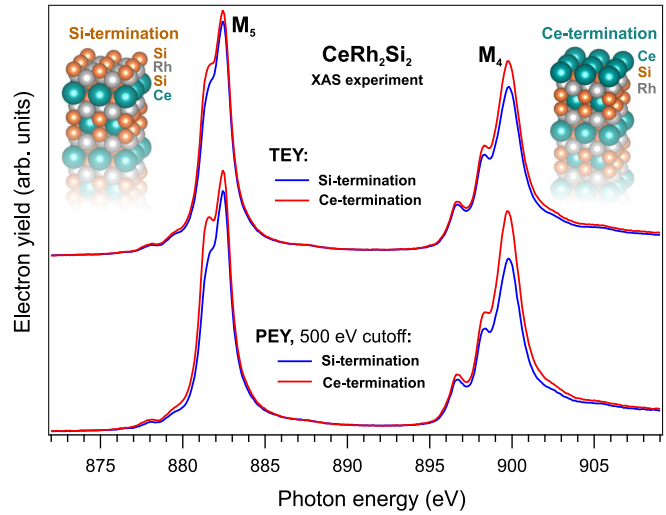

FIG. 1. Unveiling surface effects via XAS at the Ce $M_{4,5}$ edge. Experimental XAS spectra from Si- and Ce-terminated surfaces of $CeRh_2Si_2$ acquired in the TEY and PEY regimes. To enhance surface sensitivity, a 500 V bias was applied in the PEY measurements to suppress the detection of low-energy electrons.

III. RESULTS AND DISCUSSION

We begin by analyzing the experimental $M_{4,5}$ XAS spectra of Ce obtained from a freshly cleaved $CeRh_2Si_2$ crystal, focusing on its Si- and Ce-terminated surfaces. In Fig. 1, we present the obtained spectra using TEY and PEY regimes. In the latter case, to enhance the surface sensitivity of the XAS measurements, we applied a 500 V retarding voltage to suppress the contribution of low kinetic energy electrons to the acquired signal. Although XAS measurements performed in the TEY regime at the Ce $3d$ edge are traditionally considered bulk sensitive, as they primarily reflect transitions of core $3d$ electrons to the E_F region where $4f$ states dominate, we observe clear differences in the TEY spectra at both the M_5 and M_4 peak regions depending on whether the synchrotron beam illuminates the Si- or Ce-terminated surface. This indicates a detectable sensitivity of the TEY measurements to variations in surface termination and, consequently, to the surface-related properties of Ce atoms, their local environments, the properties of $4f$ magnetic moments, and interactions of $4f$ with itinerant electrons. This is in line with our recent ARPES studies of the Kondo scale properties at the surface and in the bulk of $CeRh_2Si_2$ [28]. A closer examination of the pair of PEY spectra suggests that the spectral difference observed in the TEY data is clearly systematic and becomes significantly more pronounced in the spectra taken in the PEY regime. Additionally, for the Ce-terminated surface, the differences between the TEY and PEY spectra are substantial in both the M_4 and M_5 peak regions, whereas for the Si-terminated surface, these differences are less pronounced.

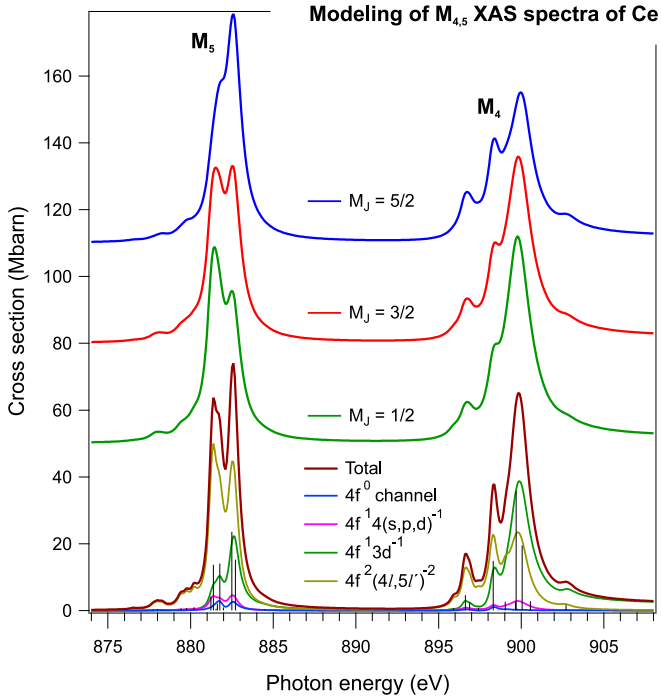

FIG. 2. Modeling of Ce $M_{4,5}$ XAS spectra. Calculated unpolarized $3d$ XAS spectrum of Ce with partial contributions from various decay channels (at the bottom). Polarized spectra for different $|M_J\rangle$ ground states and for linear photon polarization orthogonal to the quantization axis (c axis) are presented after broadening by 0.17 eV. Here and further, the energies and dipole transition probabilities for the intermediate states are illustrated with vertical lines.

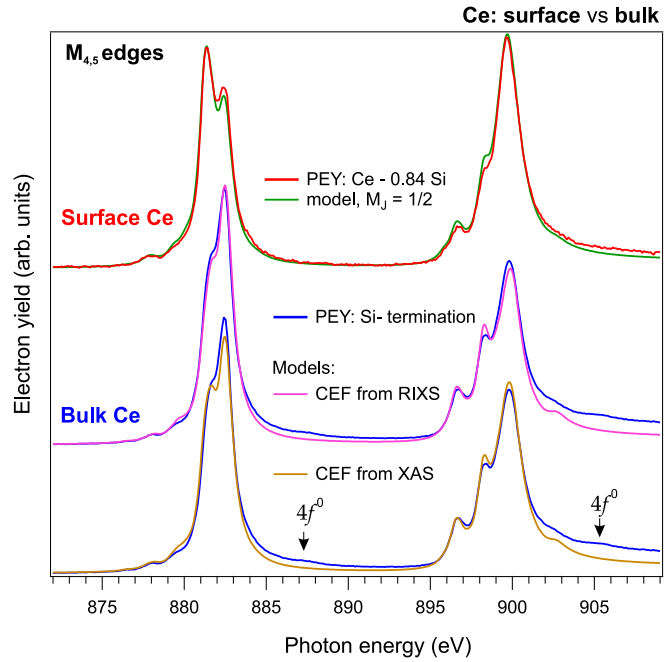

FIG. 3. Analysis of surface and bulk Ce properties via XAS: $4f$ moment reorientation. Experimental Ce XAS data taken at the $3d$ edge in the PEY mode from $CeRh_2Si_2$ at 40 K. The difference spectrum marked as "Ce-0.84Si" (shown at the top) was derived from the XAS spectra of Ce- and Si-terminated surfaces. It represents the topmost atomic layer of Ce and shows good agreement with the modeled spectrum for $M_J = 1/2$, implying a reorientation of the Ce $4f$ moments at the Ce surface compared to the bulk. The experimental spectrum from the Si termination is compared with the modeled spectra for the CEF parameters derived from RIXS [36] and XAS [14] measurements.

To gain deeper insight into the origin of the spectral changes and their relation to the properties of Ce atoms at the surface and in the bulk, we modeled the Ce XAS spectra at the $3d$ edge. The results are summarized in Fig. 2. In our modeling, we considered the photoionization of an isolated ion with a $4f^n$ ground state configuration (where $n = 1$ for Ce). The empirically adjusted parameters used in the calculations are provided in the Supplemental Material [31]. The x-ray absorption matrix element was calculated using a T-matrix approach [37]. In our calculations, we considered direct photoemission from the $4f$ and $3d$ states, as well as indirect photoemission, which involves photoexcitation from the ground $|4f^n\rangle$ configuration to the intermediate $|4f^{n+1}3d^9\rangle$ states, followed by decay through various channels.

We include an Auger channel with $|4f^{n-1}, kl\rangle$ final states, where kl indicates photoelectron with momentum k and orbital quantum number l, a decay to $|4f^n4(s, p, d)^{-1}, kl\rangle$ states, where one hole is created in one of the $4s$, $4p$, and $4d$ subshells, and a decay to $|4f^n3d^{-1}, kf\rangle$ states. We also account for the Auger channel involving final states $|4f^{n+1}(4s, 4p, 4d, 5s, 5p)^{-2}, kl\rangle$, where two holes can reside either within one subshell (e.g., $4p^4$) or in two different subshells (e.g., $4s^14p^5$). The methodology of the calculation is similar to that described in Ref. [18] and its Supplemental Material, although we additionally include the radiative decay rate as an imaginary part of the energy of intermediate states. Additional broadening of the calculated spectra (by 0.17 eV for $3d$ XAS of Ce and Pr, by 0.18 eV for Tm, and by 0.23 eV for Tb) was applied to simulate the experimental energy resolution.

Further, we present three calculated XAS spectra of Ce at the $3d$ edge for the ground states with $M_J = 1/2$, $3/2$, and $5/2$. As seen, significant differences appear at both the M_4 and M_5 edges, with the latter exhibiting a well-characterized double-peak structure, where the relative intensity of the peaks is redistributed with respect to each other depending on $|M_J\rangle$.

We now turn to the experiment, analyzing the Ce $3d$ XAS spectra obtained from the Ce- and Si-terminated surfaces of $CeRh_2Si_2$ and assessing them in relation to the calculated spectra. The top pair of spectra in Fig. 3 compares the experimental spectrum of the Ce-terminated surface (after subtraction of the bulk Ce signal) with the calculated one for $M_J = 1/2$. To extract this pure Ce-terminated surface spectrum corresponding to a single Ce layer, we subtracted the PEY spectrum of the Si-terminated surface, scaled by a factor of 0.84, from that of the Ce-terminated one. This coefficient, determined as $\exp(-d/\lambda \cos\theta)$, accounts for the attenuation of the Si-terminated crystal signal by the surface atomic layer of Ce with a thickness of $d = 1.25$ Å, using the inelastic mean free path of $\lambda = 13.8$ Å for electrons detected by the PEY detector at the emission angle of about $\theta \approx 60^\circ$. This gives an estimate of the PEY surface sensitivity defined by fast Auger

electrons when secondary electron emission is suppressed. The corresponding escape depth is approximately 7 Å. Considering the lattice parameter $c = 10.18$ Å for $CeRh_2Si_2$ [38], this implies that our PEY measurements effectively probed the topmost Ce layer as well as the next Ce layer. The latter, separated by a Si–Rh–Si block, corresponds to the fifth atomic layer below the Ce-terminated surface of $CeRh_2Si_2$. We further assume that the x-ray penetration depth remains much larger than the electron escape depth across the entire absorption edge.

As seen, the experimental and calculated spectra are in excellent agreement, implying that the ground state of the surface Ce ions is $|1/2\rangle$ (see [31] for statistical error analysis). Meanwhile, the spectrum taken from the Si-terminated surface, and which is expected to reflect the bulk-related properties of Ce in the crystal, looks quite similar to the calculated spectrum for $|M_J\rangle = 5/2$. We should note that the TEY spectrum taken from the Si surface is almost identical to the one obtained in PEY mode; therefore, it is not shown. From this, we conclude that the Ce $4f$ moments are aligned along the c direction in the bulk, as derived from the pure bulk-sensitive measurements [38], while at the surface, they clearly undergo reorientation and tend to align within the *ab* surface plane.

We note that our theoretical approach neglects any $4f$ configurational mixing, which is particularly important for Ce intermetallic compounds. In these materials, there is an admixture of $4f^0$ and $4f^2$ configurations with the dominant (trivalent) $4f^1$ configuration. The contribution from the $4f^0$ initial state is reflected as shoulders in the bulk Ce XAS spectrum, appearing around 887 eV and 905 eV. The absence of this $4f^0$ contribution in the surface Ce spectrum is consistent with the established understanding that Ce at the surface generally adopts a trivalent state, owing to reduced atomic coordination and weaker hybridization [39].

As seen, the Ce $4f$ moments in $CeRh_2Si_2$ behave similarly to the Ln $4f$ moments in other $LnRh_2Si_2$ materials, exhibiting strong reorientation at the surface compared to the bulk due to changes in CEF at the surface. We believe that this aspect should also be considered for a deeper elucidation of the unexpectedly different Kondo behavior at the surface versus the bulk, which we recently discovered [28]. In Fig. 3, we also compare the afore-discussed Ce $3d$ XAS spectra taken from the Si surface with the calculated ones obtained using the CEF parameters derived from RIXS [36] and TEY-XAS [14] measurements. In the latter case, XAS was used to determine the mixing between the $|3/2\rangle$ and $|5/2\rangle$ states. While the RIXS results proposed an almost pure $|5/2\rangle$ ground state [36], the XAS analysis suggested a significant admixture of the $|3/2\rangle$ state [14]. Our analysis suggests that CEF parameters extracted from truly bulk-sensitive RIXS measurements provide a better description of the spectrum from the Si surface. Thus it is possible to explain the discrepancy between the CEF parameters obtained with different methods by the contribution of the surface Ce atoms with $|1/2\rangle$ ground state to the XAS data. Based on this comparison, we conclude that Ce $3d$ XAS measurements remain valuable for the analysis of the ground state properties; however, to accurately derive the CEF parameters and mitigate surface-related effects, they should be complemented with other bulk-sensitive techniques.

Now, let us turn to the Ce $4d$ edge. Due to its lower photon energy, this edge exhibits a stronger surface sensitivity in XAS measurements, making it particularly sensitive to surface termination effects. As a result, clear differences in the TEY spectra between Si- and Ce-terminated surfaces should be expected. The Ce $4d \rightarrow 4f$ absorption spectrum is well known and widely used in photoemission studies to resonantly enhance emission from Ce-derived states and highlight spectral features associated with the Kondo resonance. However, a detailed analysis of the spectral shape of the Ce $4d$ XAS spectrum remains largely unexplored. In particular, no comprehensive study has examined how the pre-edge multiplet structure and the giant resonance evolve as a function of different $|M_J\rangle$ states.

We recall that $CeRh_2Si_2$ has $T_N = 38$ K and $T_K \approx 30$ K and note that all experimental results were obtained at a temperature of 40 K. Due to technical limitations, measurements were not possible at lower temperatures within the bulk AFM region. Therefore, our estimates refer to the PM phase. However, for the Si-terminated surface in the AFM regime [15,16] we expect no significant difference that would be resolvable by XAS, since the CEF levels are well separated in energy. In this case, the CEF primarily determines the orientation of the Ce $4f$ moments along the c axis. For the case of Ce termination, the ground state $|\pm 1/2\rangle$ allows us to expect orientation of the moments close to the *ab* plane in the magnetically ordered phase. Moreover, the ordering temperature at the Ce surface may differ substantially from that in the bulk [28].

Further, we address this point and the results of the XAS calculation are presented in Fig. 4. At the bottom, we show the calculated Ce $4d$ XAS spectrum, along with the contributions from different decay channels, labeled in Fig. 4. It is worth noting that the shape of Ce-$4d$-XAS spectra is material dependent, but the differences lie predominantly in the giant resonance region, while the pre-edge structures are in most cases very similar to those of trivalent CeF_3. Exceptions are the pre-edge regions of ionic tetravalent compounds such as CeO_2 and CeF_4, which consist of a simple doublet instead of a complex multiplet [40]. The reasons for the material dependence of the XAS spectra include different conduction band densities of states, crossover Auger processes, valence band interactions, and $4f$ configurational mixing. In the latter case, a tetravalent $4f^0$ admixture to a trivalent $4f^1$ configuration in the ground state is expected to result in the pre-edge structure looking like a superposition of CeF_3 and CeF_4 spectra except for linewidths. Why this is not the case is not well understood and is beyond the subject of the present manuscript. Instead, we show that the pre-edge structure can be described quantitatively on the basis of an atomic trivalent $4f^1$ state alone and thus allows statements about M_J quantum numbers and hence the orientation of the $4f$ moments in the ground state. Another reason for the material dependence of Ce $4d \rightarrow 4f$ XAS spectra is related to the ionization threshold of $4d$ electrons, which may vary between different Ce systems. In the case of $CeRh_2Si_2$, the features of the giant resonance (α and β) are significantly broader than those observed, for example, in CeF_3, which we attribute to a lower $4d$ ionization threshold that is an adjustable parameter of the calculation. The pre-edge features in $CeRh_2Si_2$ are also broader than in CeF_3, necessitating the inclusion of a small additional decay channel

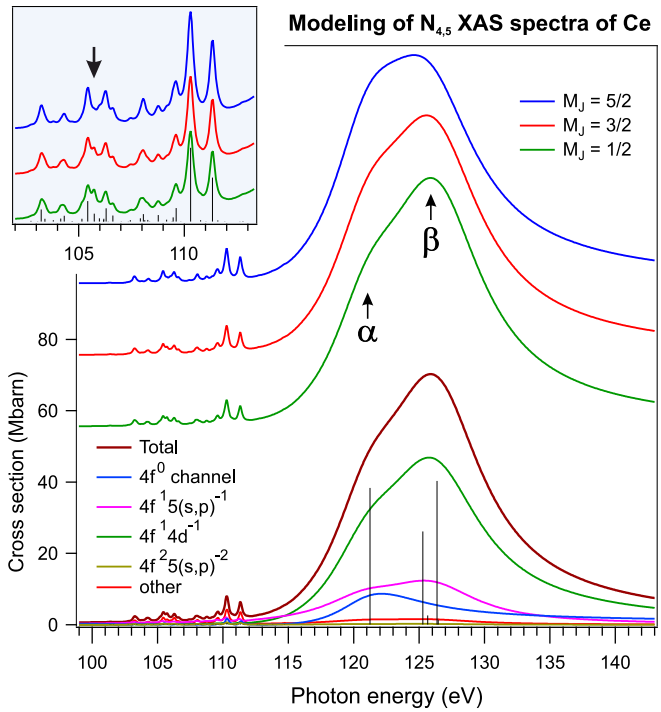

FIG. 4. Modeling of Ce $N_{4,5}$ XAS spectra. Calculated unpolarized XAS spectrum of Ce at the $N_{4,5}$ ($4d \rightarrow 4f$) edge, which includes the pre-edge multiplet structure and a giant resonance, shown at the bottom along with the contributions of different decay channels. The energies and dipole transition probabilities for the intermediate states are illustrated with vertical lines. Polarized spectra for different $|M_J\rangle$ ground states of Ce are presented for linear photon polarization orthogonal to the quantization axis c. The inset shows an enhanced view of their fine multiplet structure with the most M_J-dependent feature marked with the arrow.

(denoted as "other" channel with a decay rate of 0.1 eV for all states) accounting for decay processes involving delocalized states that are not explicitly incorporated in the model. In the upper part of Fig. 4, we present three calculated XAS spectra of Ce at the $4d$ edge for the ground states $M_J = 1/2$, $3/2$, and $5/2$. An inset magnifies the region of the pre-edge multiplet structure, indicating the fine spectral differences, marked with an arrow. A closer inspection of these results reveals notable modifications in the broad giant resonance depending on M_J, particularly in the features labeled α and β, whose intensities vary relative to each other.

In Fig. 5(a), we show TEY spectra taken exclusively from the Ce- and Si-terminated surfaces, revealing notable differences in the spectral shape, mainly of the giant resonance. In Fig. 5(b), we present the extracted XAS spectrum for the pure Ce-terminated surface and compare it with the calculated spectrum for $M_J = 1/2$. Finally, in Fig. 5(c), we compare the spectrum taken from the Si-terminated surface, which is expected to reflect the properties of Ce in the bulk, with the modeled spectrum that incorporates CEF parameters obtained from RIXS measurements. The analysis supports our conclusions drawn from the Ce XAS $3d$ spectra, with the key finding being the reorientation of Ce $4f$ moments at the Ce surface compared to the bulk. We wish to emphasize that while the spectral changes are small compared to the Ce $3d$ XAS spectra, they are notable and essential for a deeper understanding of the information derived from XAS data. We believe that a detailed analysis of the resonant ARPES data taken across the Ce $4d \rightarrow 4f$ absorption threshold together with the analysis of the XAS spectral shape may provide further insight into the Kondo-related physics associated with the CEF and the orientation of the Ce $4f$ moments.

Further, we present our findings on the antiferromagnetic compounds $TmRh_2Si_2$, $TbRh_2Si_2$, and $PrRh_2Si_2$, analyzed using the same approach as described above for $CeRh_2Si_2$. This addition is motivated by the lack of detailed information in the literature, despite the extensive investigation of lanthanide materials over several decades.

The results for $TmRh_2Si_2$ are shown in Fig. 6. The spectrum of Tm consists of only four lines. The lowest-energy peak corresponds to the state with $J = 6$, while the other

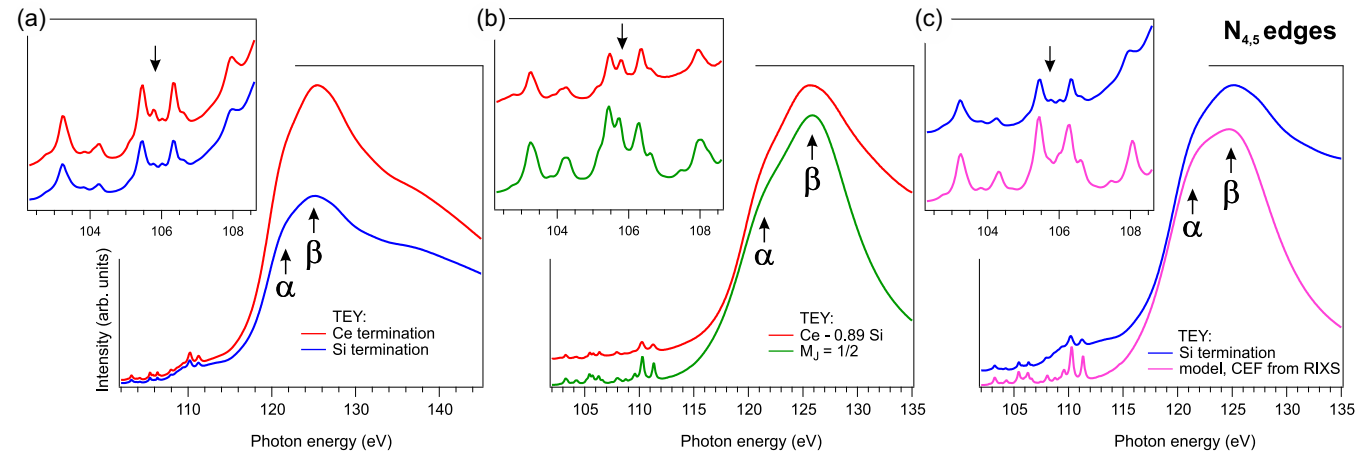

FIG. 5. Unveiling surface and bulk properties of Ce via $N_{4,5}$ XAS spectra. Experiments were performed for Ce- and Si-terminated surfaces of $CeRh_2Si_2$ at 40 K. (a) XAS spectra recorded in the TEY regime. (b) Extracted spectrum for the pure Ce-terminated surface compared with the calculated spectrum for $M_J = 1/2$. (c) Spectrum from the Si-terminated surface compared with a model spectrum with the CEF parameters derived from RIXS [36]. Insets highlight magnified regions of the pre-edge multiplet structure with the most M_J-dependent feature marked with the arrow.

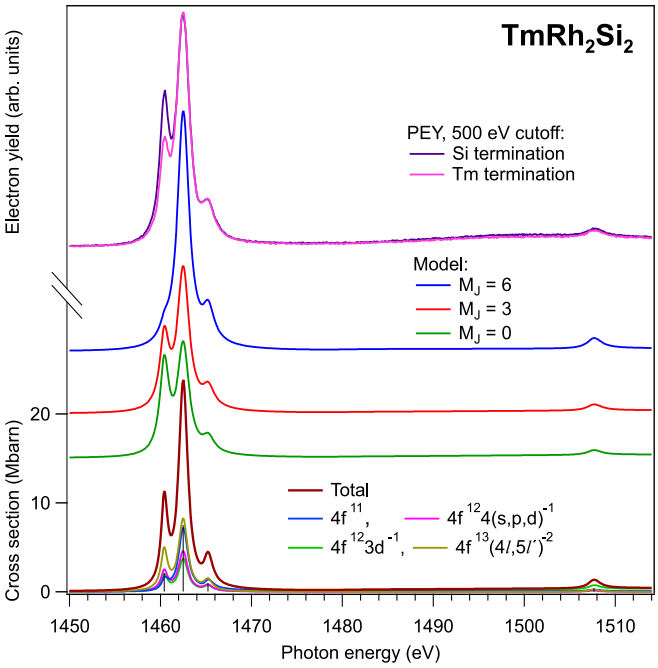

FIG. 6. Tm $M_{4,5}$ XAS spectra. Experimental data taken from the Si- and Tm-terminated surfaces of $TmRh_2Si_2$ in the PEY mode and normalized to the maximum of intensity are shown at the top. Calculated absorption cross section of a Tm^{3+} ion is given below for the unpolarized ground state and for different $|M_J\rangle$ states.

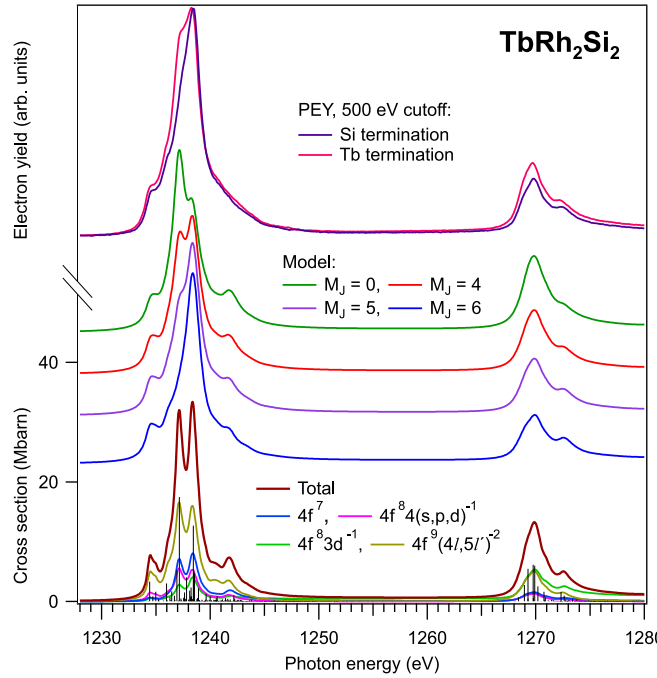

FIG. 7. Tb $M_{4,5}$ XAS spectra. Experimental data taken from the Si- and Tb-terminated surfaces of $TbRh_2Si_2$ in the PEY mode and normalized to the maximum of intensity are shown at the top. Calculated absorption cross section of a Tb^{3+} ion is given below for the unpolarized ground state and for different $|M_J\rangle$ states.

three lines have $J = 5$. Hence the model spectra of a polarized Tm ion with different $|M_J\rangle$ ground states show varying intensity ratio between the first (left) peak and the other three peaks. Such differences are well seen in the experimental XAS spectra taken from different surface terminations of $TmRh_2Si_2$, indicating that the ground state of Tm ions on the Tm-terminated surface is notably different from the ground states of Tm ions located below the surface. In particular, higher M_J values contribute to the state of the surface Tm ions. Of course, one should take into account that the surface lanthanide layer contributes only weakly to the spectrum; therefore, the differences between the spectra from two terminations are not as pronounced as between the model spectra for different M_J.

For the $TbRh_2Si_2$ crystals we obtained qualitatively similar results that are shown in Fig. 7. From the comparison of experimental spectra with the model one it becomes clear that the ground state of Tb ions located below the surface is dominated by the maximal M_J value of 6, which implies the out-of-plane orientation of the $4f$ moments. However, for the surface Tb ions the moments tend to be canted toward the in-plane direction, which is evidenced by the contributions of smaller M_J. The main difference between the cases of Tb and Tm is that for the surface Tb ions small M_J values contribute to the ground state, while for Tm large M_J values dominate. This is due to opposite signs of the CEF matrix elements related to the B_0^2 CEF parameter for Tb and Tm. For the negative B_0^2 CEF parameter, that is the case at the surface, the moments tend to be oriented in the plane for Tb (or Ce) and out of the plane for Tm.

Finally, let us consider $PrRh_2Si_2$ as illustrated in Fig. 8. Similarly to $TbRh_2Si_2$, the spectrum taken from the Si-terminated surface resembles closely the model spectrum for the largest M_J value of 4. In contrast, the spectrum from the Pr-terminated surface clearly reveals a smaller M_J.

All conclusions regarding the three systems considered with Tm, Tb, and Pr agree with the results of the analysis of $4d$ XAS spectra [18]. The most essential message of the present work is the demonstration that such surface effects are also well seen in the $3d$ spectra. Of course, the difference between the $3d$ TEY spectra taken from different terminations is rather small due to the large probing depth, but it becomes essential when a quantitative analysis of the ground state is performed on the basis of the XAS spectra. The differences become more significant in the PEY mode, although the $3d$ PEY spectra remain more bulk sensitive than the $4d$ TEY spectra.

In summary, our experiments demonstrate that surface phenomena related to lanthanide atoms near the crystal surface can be explored using conventional Ln XAS $3d$ measurements, even when performed in TEY mode, which is traditionally used for studies of bulk properties. These surface effects become significantly more pronounced in XAS spectra taken in the PEY regime. The altered coordination of Ln atoms near the surface leads to changes in the CEF, modifying the $4f$ splitting and reorienting the $4f$ moments, which in turn may drive a dramatic modification of the magnetic properties at the surface compared to the bulk.

We focus on the $CeRh_2Si_2$ compound, utilizing XAS measurements at both the $4d$ and $3d$ edges, to establish a methodology for studying $4f$-driven physics at both the

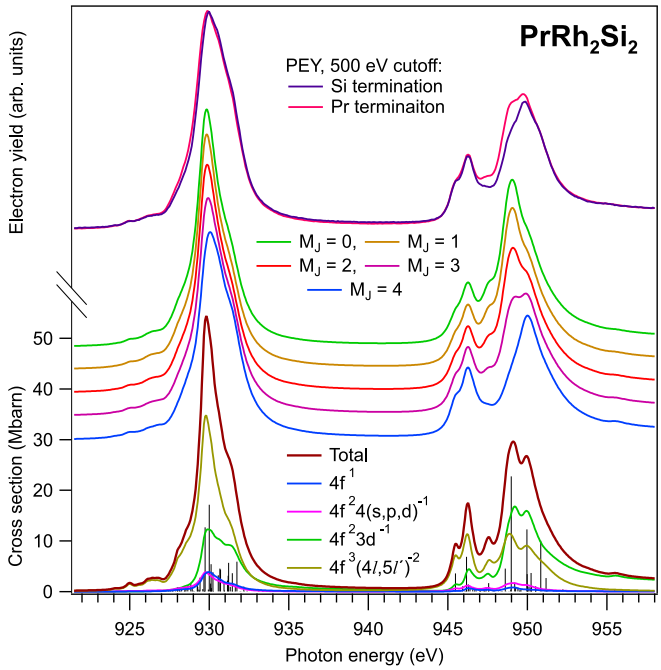

FIG. 8. Pr $M_{4,5}$ XAS spectra. Experimental data taken from the Si- and Tm-terminated surfaces of $PrRh_2Si_2$ in the PEY mode and normalized to the maximum of intensity are shown at the top. Calculated absorption cross section of a Pr^{3+} ion is given below for the unpolarized ground state and for different $|M_J\rangle$ states.

surface and bulk. A key finding of our work is the clear observation of a reorientation of Ce $4f$ magnetic moments near the surface, driven by changes in the CEF. Despite decades of research on Ce-based compounds, this surface-induced reorientation of Ce $4f$ moments has not been widely recognized, though it plays a significant role in Kondo-related physics. We argue that this phenomenon must be considered when interpreting spectroscopic studies of Ce-based systems, particularly those employing surface-sensitive photon-in electron-out techniques such as ARPES and XAS, both retrospectively and in future investigations. Thus our story carries an instructive point as well: surface-related phenomena must always be carefully disentangled from bulk properties, even in the TEY regime of XAS, as neglecting this distinction may lead to misleading conclusions.

Furthermore, by including XAS $3d$ data from $TmRh_2Si_2$, $PrRh_2Si_2$, and $TbRh_2Si_2$, we offer a broader perspective on the importance of surface effects in bulk-sensitive XAS measurements. This provides a more comprehensive understanding of the role of surface phenomena in lanthanide materials. We suggest that future research should explore how the interactions between magnetically active $3d$ and $4f$ sublattices evolve from the bulk to the surface. Such investigations may reveal Kondo-driven phenomena and emergent magnetic order in low-dimensional systems.

ACKNOWLEDGMENTS

We acknowledge the German Research Foundation (DFG) for the support of our research through Grants No. GU2228/2-1 (Project No. 512344413) and TRR288 (No. 422213477, Project No. A03). The authors acknowledge Saint-Petersburg State University for a research Project No. 125022702939-2. The work of D.Yu.U. (modeling of XAS spectra) was supported by the Ministry of Science and Higher Education of the Russian Federation (Grant No. 075-15-2025-010 from 28.02.2025). The work of V.S.S. (analysis of experimental XAS data) was supported by RSF Grant No. 23-72-30004. We acknowledge MAX IV Laboratory for experimental time on FlexPES beamline [29] under Proposals No. 20240575 and No. 20230457. Research conducted at MAX IV, a Swedish national user facility, is supported by the Swedish Research Council under Contract No. 2018-07152, the Swedish Governmental Agency for Innovation Systems under Contract No. 2018-04969, and Formas under Contract No. 2019-0249. We are grateful to A. Preobrajenski and A. Generalov, staff members at the FlexPES facility [29], for their strong interest and support of this research, exceptional management of the FlexPES, and valuable discussions throughout the preparation of this paper. We also thank C. Laubschat for his valuable interest in this work and fruitful discussions.

DATA AVAILABILITY

The data that support the findings of this article are not publicly available upon publication because it is not technically feasible and/or the cost of preparing, depositing, and hosting the data would be prohibitive within the terms of this research project. The data are available from the authors upon reasonable request.

[1] J. Stöhr, *NEXAFS Spectroscopy*, Springer Series in Surface Sciences (Springer-Verlag, Berlin, Heidelberg, 1992), Vol. 25.

[2] B. T. Thole, G. van der Laan, J. C. Fuggle, G. A. Sawatzky, R. C. Karnatak, and J.-M. Esteva, 3d x-ray-absorption lines and the $3d^9 4f^{n+1}$ multiplets of the lanthanides, Phys. Rev. B **32**, 5107 (1985).

[3] *X-Ray Absorption and X-Ray Emission Spectroscopy: Theory and Applications*, edited by J. A. van Bokhoven and C. Lamberti (Wiley, New York, 2016), Vol. 1-2.

[4] *Handbook on the Physics and Chemistry of Rare Earths, Volume 37*, edited by K. A. Gschneidner, J.-C. G. Bünzli, and V. K. Pecharsky (Elsevier, Amsterdam, 2007).

[5] *Spectroscopic Properties of Rare Earths in Optical Materials*, edited by G. Liu and B. Jacquier, Springer Series in Materials Science (Springer, Berlin, 2005), Vol. 83.

[6] *The Rare Earth Elements: Fundamentals and Applications*, edited by D. A. Atwood (John Wiley & Sons, Chichester, West Sussex, UK, 2012).

[7] G. R. Stewart, Non-fermi-liquid behavior in d- and f-electron metals, Rev. Mod. Phys. **73**, 797 (2001).

[8] G. R. Stewart, Addendum: Non-fermi-liquid behavior in d- and f-electron metals, Rev. Mod. Phys. **78**, 743 (2006).

[9] P. Hansmann, A. Severing, Z. Hu, M. W. Haverkort, C. F. Chang, S. Klein, A. Tanaka, H. H. Hsieh, H.-J. Lin, C. T. Chen,

B. Fåk, P. Lejay, and L. H. Tjeng, Determining the crystal-field ground state in rare earth heavy fermion materials using soft-x-ray absorption spectroscopy, Phys. Rev. Lett. **100**, 066405 (2008).

[10] T. Willers, B. Fåk, N. Hollmann, P. O. Körner, Z. Hu, A. Tanaka, D. Schmitz, M. Enderle, G. Lapertot, L. H. Tjeng, and A. Severing, Crystal-field ground state of the noncentrosymmetric superconductor $CePt_3Si$: A combined polarized soft x-ray absorption and polarized neutron study, Phys. Rev. B **80**, 115106 (2009).

[11] F. Strigari, T. Willers, Y. Muro, K. Yutani, T. Takabatake, Z. Hu, Y.-Y. Chin, S. Agrestini, H.-J. Lin, C. T. Chen, A. Tanaka, M. W. Haverkort, L. H. Tjeng, and A. Severing, Crystal-field ground state of the orthorhombic Kondo insulator $CeRu_2Al_{10}$, Phys. Rev. B **86**, 081105(R) (2012).

[12] A. Amorese, P. Hansmann, A. Marino, P. Körner, T. Willers, A. Walters, K.-J. Zhou, K. Kummer, N. B. Brookes, H.-J. Lin, C.-T. Chen, P. Lejay, M. W. Haverkort, L. H. Tjeng, and A. Severing, Orbital selective coupling in $CeRh_3B_2$: Coexistence of high Curie and high Kondo temperatures, Phys. Rev. B **107**, 115164 (2023).

[13] D. S. Christovam, M. Ferreira-Carvalho, A. Marino, M. Sundermann, D. Takegami, A. Melendez-Sans, K. D. Tsuei, Z. Hu, S. Rößler, M. Valvidares, M. W. Haverkort, Y. Liu, E. D. Bauer, L. H. Tjeng, G. Zwicknagl, and A. Severing, Spectroscopic evidence of Kondo-induced quasiquartet in $CeRh_2As_2$, Phys. Rev. Lett. **132**, 046401 (2024).

[14] T. Willers, D. T. Adroja, B. D. Rainford, Z. Hu, N. Hollmann, P. O. Körner, Y.-Y. Chin, D. Schmitz, H. H. Hsieh, H.-J. Lin, C. T. Chen, E. D. Bauer, J. L. Sarrao, K. J. McClellan, D. Byler, C. Geibel, F. Steglich, H. Aoki, P. Lejay, A. Tanaka, L. H. Tjeng, and A. Severing, Spectroscopic determination of crystal-field levels in $CeRh_2Si_2$ and $CeRu_2Si_2$ and of the $4f^0$ contributions in CeM_2Si_2 (M = Cu, Ru, Rh, Pd, and Au), Phys. Rev. B **85**, 035117 (2012).

[15] D. Y. Usachov, D. Glazkova, A. V. Tarasov, S. Schulz, G. Poelchen, K. A. Bokai, O. Y. Vilkov, P. Dudin, K. Kummer, K. Kliemt, C. Krellner, and D. V. Vyalikh, Estimating the orientation of $4f$ magnetic moments by classical photoemission, J. Phys. Chem. Lett. **13**, 7861 (2022).

[16] A. V. Tarasov, D. Glazkova, S. Schulz, G. Poelchen, K. Kliemt, A. Kraiker, M. Muntwiler, C. Laubschat, A. Generalov, C. Polley, C. Krellner, D. V. Vyalikh, and D. Y. Usachov, Crystal electric field and properties of $4f$ magnetic moments at the surface of the rare-earth compound $TbRh_2Si_2$, Phys. Rev. B **106**, 155136 (2022).

[17] D. Y. Usachov, A. V. Tarasov, D. Glazkova, M. Mende, S. Schulz, G. Poelchen, A. V. Fedorov, O. Y. Vilkov, K. A. Bokai, V. S. Stolyarov, K. Kliemt, C. Krellner, and D. V. Vyalikh, Insight into the temperature-dependent canting of 4f magnetic moments from 4f photoemission, J. Phys. Chem. Lett. **14**, 5537 (2023).

[18] D. Y. Usachov, K. A. Bokai, I. I. Klimovskikh, K. Ali, F. Schiller, G. Poelchen, V. S. Stolyarov, K. Kliemt, C. Krellner, and D. V. Vyalikh, Probing surface and bulk ground states of lanthanides: $4f$ moment orientation through $4d$ x-ray absorption spectroscopy, Phys. Rev. B **110**, 075157 (2024).

[19] H. Moriya, H. Tsuchiura, and A. Sakuma, First principles calculation of crystal field parameter near surfaces, J. Appl. Phys. **105**, 07A740 (2009).

[20] H. Tsuchiura, T. Yoshioka, and P. Novák, Bridging atomistic magnetism and coercivity in Nd-Fe-B magnets, Scr. Mater. **157**, 69 (2018).

[21] H. Tsuchiura, T. Yoshioka, P. Novák, J. Fischbacher, A. Kovacs, and T. Schrefl, First-principles calculations of magnetic properties for analysis of magnetization processes in rare-earth permanent magnets, Sci. Technol. Adv. Mater. **22**, 748 (2021).

[22] R. Movshovich, T. Graf, D. Mandrus, J. D. Thompson, J. L. Smith, and Z. Fisk, Superconductivity in heavy-fermion $CeRh_2Si_2$, Phys. Rev. B **53**, 8241 (1996).

[23] S. Araki, M. Nakashima, R. Settai, T. C. Kobayashi, and Y. Onuki, Pressure-induced superconductivity in an antiferromagnet $CeRh_2Si_2$, J. Phys.: Condens. Matter **14**, L377 (2002).

[24] W. Knafo, D. Aoki, D. Vignolles, B. Vignolle, Y. Klein, C. Jaudet, A. Villaume, C. Proust, and J. Flouquet, High-field metamagnetism in the antiferromagnet $CeRh_2Si_2$, Phys. Rev. B **81**, 094403 (2010).

[25] K. Götze, D. Aoki, F. Lévy-Bertrand, H. Harima, and I. Sheikin, Drastic change of the Fermi surface across the metamagnetic transition in $CeRh_2Si_2$, Phys. Rev. B **95**, 161107(R) (2017).

[26] W. Knafo, R. Settai, D. Braithwaite, S. Kurahashi, D. Aoki, and J. Flouquet, Three-dimensional critical phase diagram of the Ising antiferromagnet $CeRh_2Si_2$ under intense magnetic field and pressure, Phys. Rev. B **95**, 014411 (2017).

[27] S. Patil, A. Generalov, M. Güttler, P. Kushwaha, A. Chikina, K. Kummer, T. C. Rödel, A. F. Santander-Syro, N. Caroca-Canales, C. Geibel, S. Danzenbächer, Y. Kucherenko, C. Laubschat, J. W. Allen, and D. V. Vyalikh, ARPES view on surface and bulk hybridization phenomena in the antiferromagnetic Kondo lattice $CeRh_2Si_2$, Nat. Commun. **7**, 11029 (2016).

[28] G. Poelchen, S. Schulz, M. Mende, M. Güttler, a. Generalov, A. V. Fedorov, N. Caroca-Canales, C. Geibel, K. Kliemt, C. Krellner, S. Danzenbächer, D. Y. Usachov, P. Dudin, V. N. Antonov, J. W. Allen, C. Laubschat, K. Kummer, Y. Kucherenko, and D. V. Vyalikh, Unexpected differences between surface and bulk spectroscopic and implied Kondo properties of heavy fermion $CeRh_2Si_2$, npj Quantum Mater. **5**, 70 (2020).

[29] A. Preobrajenski, A. Generalov, G. Öhrwall, M. Tchaplyguine, H. Tarawneh, S. Appelfeller, E. Frampton, and N. Walsh, FlexPES: a versatile soft X-ray beamline at MAX IV Laboratory, J. Synch. Rad. **30**, 831 (2023).

[30] K. Kliemt, M. Peters, F. Feldmann, A. Kraiker, D.-M. Tran, S. Rongstock, J. Hellwig, S. Witt, M. Bolte, and C. Krellner, Crystal growth of materials with the $ThCr_2Si_2$ structure type, Cryst. Res. Technol. **55**, 1900116 (2020).

[31] See Supplemental Material at http://link.aps.org/supplemental/10.1103/blg4-bxl5 for additional information about the ARPES characterization of the surface terminations of the cleaved surface of $CeRh_2Si_2$, as well as the details of the XAS calculation parameters.

[32] M. Güttler, K. Kummer, S. Patil, M. Höppner, A. Hannaske, S. Danzenbächer, M. Shi, M. Radovic, E. Rienks, C. Laubschat, C. Geibel, and D. V. Vyalikh, Tracing the localization of $4f$ electrons: Angle-resolved photoemission on $YbCo_2Si_2$, the stable trivalent counterpart of the heavy-fermion $YbRh_2Si_2$, Phys. Rev. B **90**, 195138 (2014).

[33] D. Y. Usachov, I. A. Nechaev, G. Poelchen, M. Güttler, E. E. Krasovskii, S. Schulz, A. Generalov, K. Kliemt, A. Kraiker, C. Krellner, K. Kummer, S. Danzenbächer, C. Laubschat,

A. P. Weber, J. Sánchez-Barriga, E. V. Chulkov, A. F. Santander-Syro, T. Imai, K. Miyamoto, T. Okuda, and D. V. Vyalikh, Cubic Rashba effect in the surface spin structure of rare-earth ternary materials, Phys. Rev. Lett. **124**, 237202 (2020).

[34] M. Güttler, A. Generalov, M. M. Otrokov, K. Kummer, K. Kliemt, A. Fedorov, A. Chikina, S. Danzenbächer, S. Schulz, E. V. Chulkov, Y. M. Koroteev, N. Caroca-Canales, M. Shi, M. Radovic, C. Geibel, C. Laubschat, P. Dudin, T. K. Kim, M. Hoesch, C. Krellner, and D. V. Vyalikh, Robust and tunable itinerant ferromagnetism at the silicon surface of the antiferromagnet $GdRh_2Si_2$, Sci. Rep. **6**, 24254 (2016).

[35] A. Generalov, M. M. Otrokov, A. Chikina, K. Kliemt, K. Kummer, M. Höppner, M. Güttler, S. Seiro, A. Fedorov, S. Schulz, S. Danzenbächer, E. V. Chulkov, C. Geibel, C. Laubschat, P. Dudin, M. Hoesch, T. Kim, M. Radovic, M. Shi, N. C. Plumb, C. Krellner, and D. V. Vyalikh, Spin Orientation of two-dimensional electrons driven by temperature-tunable competition of spin-orbit and exchange-magnetic interactions, Nano Lett. **17**, 811 (2017).

[36] A. Amorese, N. Caroca-Canales, S. Seiro, C. Krellner, G. Ghiringhelli, N. B. Brookes, D. V. Vyalikh, C. Geibel, and K. Kummer, Crystal electric field in $CeRh_2Si_2$ studied with high-resolution resonant inelastic soft x-ray scattering, Phys. Rev. B **97**, 245130 (2018).

[37] H. Ogasawara and A. Kotani, Calculation of rare-earth 4*d* giant-absorption spectra with multiplet effects and decay processes, J. Synchrotron Rad. **8**, 220 (2001).

[38] B. H. Grier, J. M. Lawrence, V. Murgai, and R. D. Parks, Magnetic ordering in CeM_2Si_2 (M = Ag, Au, Pd, Rh) compounds as studied by neutron diffraction, Phys. Rev. B **29**, 2664 (1984).

[39] J. W. Allen, The Kondo resonance in electron spectroscopy, J. Phys. Soc. Jpn. **74**, 34 (2005).

[40] G. Kalkowski, C. Laubschat, W. D. Brewer, E. V. Sampathkumaran, M. Domke, and G. Kaindl, Nature of Ce $4f$ electronic states from $4d$ excitations in metals and insulators, Phys. Rev. B **32**, 2717 (1985).